Trojan Stars in the Galactic Center

M. Fujii[1,3], M. Iwasawa[2,3], Y. Funato[2], and J. Makino[3]

ABSTRACT

We performed, for the first time, the simulation of spiral-in of a star cluster formed close to the Galactic center (GC) using a fully self-consistent N-body model. In our model, the central super-massive black hole (SMBH) is surrounded by stars and the star cluster. Not only are the orbits of stars and the cluster stars integrated self-consistently, but the stellar evolution, collisions and merging of the cluster stars are also included. We found that an intermediate-mass black hole (IMBH) is formed in the star cluster and stars escaped from the cluster are captured into a 1:1 mean motion resonance with the IMBH. These "Trojan" stars are brought close to the SMBH by the IMBH, which spirals into the GC due to the dynamical friction. Our results show that, once the IMBH is formed, it brings the massive stars to the vicinity of the central SMBH even after the star cluster itself is disrupted. Stars carried by the IMBH form a disk similar to the observed disks and the core of the cluster including the IMBH has properties similar to those of IRS13E, which is a compact assembly of several young stars.

Subject headings: galaxy: star clusters — Galaxy: center, kinematics and dynamics — methods: numerical — stellar dynamics

1. Introduction

Young and massive stars have been found within one parsec from the Galactic center (GC) (Krabbe et al. 1995; Paumard et al. 2006). Some of them are ∼1000 AU from the central SMBH. How these massive stars were brought to the vicinity of the SMBH has been a mystery. One possible scenario is the following. A star cluster formed at a few tens of pc from the GC, and then spiraled in due to the dynamical friction (Gerhard 2001). Previous simulations (Portegies Zwart et al. 2003; Kim & Morris 2003; Kim et al. 2004; Gürkan & Rasio 2005) have shown that the timescale of spiral-in of the star cluster can be short enough. However, how close the stars can actually approach the SMBH is not clear.

Another possible scenario is the in-situ formation in an accretion disk (Levin & Beloborodov 2003; Nayakshin et al. 2007; Hobbs & Nayakshin 2008). Giant molecular clouds fall into the GC and form massive gaseous disks around the central BH. Stars form in the disk if it becomes gravitationally unstable and results in fragmentation. However, accretion disks have difficulty producing stars with eccentric orbits and a compact assembly of stars like IRS 13E, which is located at $\sim$ 0.13 pc in projection from the GC and contains half a dozen young stars and probably an IMBH (Hansen & Milosavljević 2003; Maillard et al. 2004). Mapelli et al. (2008) argued that if a gas cloud undergoes a very close encounter (pericenter distance of 0.01 pc) with the central SMBH, the tidal compression could trigger the star formation, resulting in stars in close, bound orbits. However, how a cloud can come that close to the GC is not clear. On the other hand, if the star cluster has an eccentric orbit, the orbits of stars escaped from the cluster are also eccentric. The remnant of the core looks like IRS 13E.

[1]Department of Astronomy, Graduate School of Science, The University of Tokyo, 7-3-1 Hongo, Bunkyo, Tokyo 113-0033; fujii@cfca.jp

[2]Department of General System Studies, College of Arts and Sciences, The University of Tokyo, 3-8-1 Komaba, Meguro, Tokyo 153-8902; iwasawa@cfca.ac.jp, funato@artcompsci.org

[3]Division of Theoretical Astronomy, National Astronomical Observatory of Japan, 2-21-1 Osawa, Mitaka, Tokyo, 181-8588; makino@cfca.jp

We performed a fully self-consistent N-body simulation in which the internal dynamics of the cluster, that of the parent galaxy, and interactions between cluster stars and galaxy stars are correctly handled. In previous simulations, when the internal dynamics was followed by an accurate N-body code, the parent galaxy had to be modeled as a fixed potential with some fitting formulae for the dynamical friction. This means that the orbital evolution is not accurate. Fujii et al. (2008) showed that the actual orbital decay of the cluster is faster than that of previous simulations and the main reason is stars with a mass grater than 90% of an initial cluster escaping from this cluster.

We describe the method of our N-body simulation in section 2. In section 3 we show the results of simulations. Section 4 is for summary.

2. Method

2.1. Models and Initial Conditions

We adopted two models for the galactic center. For both values, we adopted a model based on a King model with the non-dimensional central potential $W_0 = 10$ as galaxy models. We placed the central SMBH with the mass of $3.6 \times 10^6 M_\odot$ (Eisenhauer et al. 2005) and our galaxy models represent the central region of our Galaxy (see figure 1). The difference between two models corresponds to the initial position of a star cluster. One (GL) is for a run with the initial position of the cluster 12.5 pc from the GC, and the other (GS) 5 pc from the GC. Their total masses on the real scale (excluding the SMBH) are $5.9 \times 10^7 M_\odot$ and $2.9 \times 10^7 M_\odot$, respectively. The number of particles is 2×10^6 for both models. GS has better mass-resolution, but a smaller half-mass radius of 9.6 pc. GL has a larger half-mass radius of 22 pc for the farther initial position of the cluster. These models are summarized in table 1.

As a model of a star cluster, we adopted a King model with non-dimensional central potential of $W_0 = 6$. For runs from the initial distance of 12.5 pc from the GC, we used a model with 64k particles and the total mass of $2.1 \times 10^5 M_\odot$ (SC64k). For runs from 5pc, we used a model with 32k particles and the total mass of $1.0 \times 10^5 M_\odot$ (SC32k). Initial mass function of stars in the clusters is a Salpeter with lower and upper cutoff at 1 and 100 $M_\odot$ (Salpeter 1955). We assigned each star a mass randomly chosen from the Salpeter initial mass function, irrespective of its position. The tidal radii of the models are 1.1 pc for SC64k and 0.65 pc for SC32k. They are smaller than the tidal limits at their initial positions. The cluster models are summarized in table 2.

2.2. N-body Simulation

We used the Bridge code (Fujii et al. 2007) to handle the interaction between the parent galaxy and the star cluster fully self-consistently. The Bridge scheme is a tree-direct hybrid scheme. Only the internal motion of the star cluster is calculated by the direct scheme with high accuracy, and all other interactions are calculated by the tree algorithm. The splitting between the direct part and tree part is through the splitting of the Hamiltonian in a way similar to the mixed variable symplectic (Kinoshita, Yoshida, & Nakai 1991; Wisdom & Holman 1991). With the Bridge scheme, we can treat a large-N system with embedded small-scale systems fully self-consistently and accurately.

We used two sets of numerical parameters for each galaxy model. They are summarized in table 3. In our model, the softening length between galaxy particles and the SMBH is 0.2 pc. Therefore, our simulation has the resolution limit around 0.2 pc for the motion of the star cluster and cluster stars within the parent galaxy. We used the opening angle $\theta = 0.75$ with the center-of-mass approximation for the tree. The simulation is performed using GRAPE6 (Makino et al. 2003).

2.3. Stellar Collisions and Evolutions

In our simulation, we adopted collisions of stars in a star cluster and formation of an IMBH in the cluster. Recent simulations showed that in a dense star cluster, runaway collisions of stars form a very massive star (Portegies Zwart et al. 1999; Portegies Zwart & McMillan 2002; Portegies Zwart et al. 2004; Freitag et al. 2006). If it is massive enough, it will collapse into an IMBH (Fryer et al. 2001; Heger et al. 2003). While the massive star grows through collisions, it loses its mass due to the stellar wind. Very massive stars lose their mass rapidly (Belkus et al. 2007). However, these processes are not well understood for stars more mas-

sive than $1000M_\odot$. Therefore, we treated the collision criterion and the mass-loss rate as parameters. In this section, we describe our model of stellar collision and evolution and discuss the difference caused by these parameters.

If the core collapse occurs in the star cluster, collisions between stars in the core occur rather frequently. We let two stars merge in the star cluster if they approach to twice the sum of stellar radii, which is also adopted in Portegies Zwart et al. (1999). If two stars approach, the tidal capture occurs: the tidal force exerts stellar oscillations and the stars lose their orbital energy and become binary (Fabian et al. 1975; Press & Teukolsky 1977; McMillan et al. 1987). The critical distance for the tidal capture is around 3-4 times the radius of the star for two identical stars. When a tidally captured binary is actually formed, it would merge fairly quickly because of perturbations from nearby stars. For the radii of stars, we adopted the result of Hurley et al. (2000) (here after HPT00). The structure of very massive stars with $100 < M < 1000M_\odot$ is investigated by Ishii et al. (1999) and Yungelson et al. (2008), while that of stars more massive than $1000M_\odot$ is not. We used the results of HPT00 for very massive stars with $> 100M_\odot$. Massive stars ($> 100M_\odot$) have a core-halo structure (Ishii et al. 1999). The result of HPT00 we adopted is close to the size of the core in Ishii et al. (1999). Therefore, we adopted twice the sum of the radii as the collision criterion. To see the effect of the different criterion, we also performed simulations using the sum of the stellar radii as the collision criterion (Portegies Zwart & McMillan 2002; Portegies Zwart et al. 2004; Freitag et al. 2006).

We also take into account the mass loss due to the stellar wind for very massive stars. Belkus et al. (2007) have investigated the mass-loss rate for massive stars with $< 1000M_\odot$. However, the stellar evolution of stars with $> 1000M_\odot$ is not well understood. Furthermore, merged stars show a evolution different from that of single stars (Suzuki et al. 2007). Therefore, we treat the mass-loss rate as a parameter.

Our model for the stellar wind is based on line-driven winds developed by Castor et al. (1975; hereafter CAK). We used the formalism of Owocki et al. (2004). The mass-loss rate of the CAK model is given by

$$\dot{M}_* = \frac{L_*}{c^2}\frac{\alpha}{1-\alpha}\left[\frac{\bar{Q}\Gamma_e}{1-\Gamma_e}\right]^{(1-\alpha)/\alpha}, \quad (1)$$

where L_* is the luminosity of the star, Γ_e is the Eddington parameter, and α and $\bar{Q}$ are the power index and normalization of the line opacity distribution. The Eddington parameter is given by

$$\Gamma_e = \frac{\kappa_e L_*}{4\pi G M_* c}, \quad (2)$$

where M_* is the mass of the star, G is the gravitational constant, c is the speed of light, and κ_e is the opacity. For fully ionized plasmas with hydrogen mass fraction X, the opacity is given by $\kappa = 0.2(1+X)$ cm^2 g^{-1}, where we assumed $X = 0.7$. For very massive stars, the luminosity is proportional to the mass because in such massive stars, the contribution of radiation to the total pressure is very large (Marigo et al. 2003). Hence, we assumed $\dot{M}_* \propto M_*$, here M_* is the mass of the star. We adopted $\alpha = 0.5$(CAK), $\bar{Q} = 10^3$ (Gayley 1995), $L_* = 3.2\times10^4(M_*/M_\odot)(L_\odot)$ (Suzuki, private communication), which is close to the Eddington luminosity. From these values, we obtained

$$\dot{M}_* = 9.66\times10^{-8}\left(\frac{M_*}{M_\odot}\right)(M_\odot/\mathrm{yr}). \quad (3)$$

On the other hand, the recent results (Belkus et al. 2007) show a higher mass-loss rate. Therefore, we also adopted a mass-loss rate five times higher, similar to the result of Belkus et al. (2007). The evolution of the mass for stars with 1000 $M_\odot$ initial mass is shown in figure 2. We neglected the mass loss of the stars less than 300 $M_\odot$ because they are small enough.

We assumed that very massive stars formed by runaway collisions form black holes (BHs) at the end of their main-sequence lifetime (Fryer et al. 2001; Heger et al. 2003). For the lifetime, we adopted the results of HPT00 for stars with masses less than 100 $M_\odot$, interpolated the results of Belkus et al. (2007) for stars with masses up to 1000 $M_\odot$, and extrapolated them for more than 1000 $M_\odot$. We assigned new ages to stars born by stellar collisions using the following formalism of Meurs & van den Heuvel (1989):

$$t_{\rm age}(m_1+m_2) = \frac{m_1}{m_1+m_2}\frac{\tau_{\rm ms}(m_1+m_2)}{\tau_{\rm ms}(m_1)}t_{\rm age}(m_1), \quad (4)$$

where m_1 and m_2 are the masses of stars ($m_1 > m_2$), $t_{\rm age}$ is the age of the star, and $\tau_{\rm ms}$ is the main-sequence lifetime. The new star looks rejuvenated. However, the assumption used to derive equation (4) is that the convection core of the primary will occupy the core of the merger with the mass and composition unchanged. Suzuki et al. (2007) and also Gaburov et al. (2008) found that in the case of unequal-mass merger the core of the secondary will first occupy the center of the merger, resulting in significant mixing-in of hydrogen into the new convection core. So equation (4) might underestimate the lifetime of the merger. We assumed that the massive star directly collapses to an BH. The final evolution of the very massive star depends on its helium core mass at the end of its life. If it is more massive than $\sim 130 M_\odot$, it collapses directly to an BH without mass loss (Fryer et al. 2001).

We performed simulation for isolated star clusters and investigated the difference caused by the parameters. The model of star cluster is SC64k. The runs are summarized in table 4. Each parameter has two values. The results are shown in figure 3. The difference due to $r_{\rm coll}$ is smaller than that due to the mass-loss rate because the stellar radii is smaller than the radius, but it becomes larger when the mass grows. The mass-loss rate significantly affects the final mass. In any case, however, the mass accretion rate due to stellar collisions was higher or almost the same as the mass-loss rate. The mass loss will not prevent the formation of an IMBH in the star cluster.

2.4. Runs

We performed fully self-consistent N-body simulations of a star cluster and its parent galaxy system. Runs are summarized in table 5. For the mass-loss rate and collision criterion, we adopted two extreme cases. They are upper and lower limits of the mass of IMBHs.

3. Results

3.1. Evolution of Star Cluster and IMBH

The orbit of the star cluster decayed due to the dynamical friction and the cluster was disrupted by the tidal force. The evolutions of star clusters are shown in figure 4. Top and middle panels show the orbital and bound-mass evolution of the star clusters. Bottom panels show the mass of the most massive star in the star cluster. Black points in the bottom panels show the times when IMBHs formed.

In each case, when the pericenter distance becomes less than 2 pc, the star clusters are almost completely disrupted. The disruption time, $r_{\rm dis}$, is summarized in table 6. We defined the disruption as the time when the number of stars bound to the cluster becomes less than ten.

Before the cluster was completely disrupted, an IMBH formed in the cluster through the runaway collisions of stars. A massive star grew via repeated collisions and finally the mass of the massive star reached 3000-16000 $M_\odot$. The evolution of the massive star is shown in bottom panels of figure 4. The IMBH mass strongly depends on the mass-loss rate. The time when the IMBH formed was earlier than the disruption time except for the run HS32k. These results are summarized in table 5.

After the disruption of the star cluster, the IMBH formed sinks into the GC on the time scale of the Chandrasekhar dynamical friction (Chandrasekhar 1943). The time scale of the orbital evolution due to the dynamical friction is proportional to the mass of the star cluster (IMBH). The IMBH mass of LD64k is around three times more massive than that of HS64k. The orbital evolution of LD64k is roughly three times faster than that of HS64k. On the other hand, the orbital decay of the cluster looks faster than the time scale. This is because the dynamical friction was enhanced due to the stars escaping from the cluster (Fujii et al. 2006).

The orbital evolution of the star cluster became slower and slower at the end of the simulation. This is because we adopted a large softening length between the SMBH and galaxy particle, which is 0.2 pc. If the softening length were smaller, the cluster would approach closer to the GC and carry resonant stars. We will perform a simulation with a smaller softening length and report the results in a forthcoming paper.

Figure 5 shows the projected distribution of stars at the end of the run (7.25Myrs) of LD64k. Only stars which were originally members of the star cluster are plotted. The arrows in the right panel show the proper motions of the stars. Red ones move clockwise and green ones move coun-

terclockwise. This figure looks very similar to K-band images of the GC (cf. Lu et al. 2006, figure 2). In particular, they reached a distance of ~ 0.2 pc from the GC. We can see that, even though the cluster is almost completely disrupted at 2pc, there are a number of stars which were brought much closer to the central SMBH.

3.2. Trojan Stars

We found that many stars were carried near the GC though almost all stars became unbound at around 1-2 pc from the GC. Figure 6 shows how these stars were brought near the central SMBH. Red solid curves show the orbit of the star cluster. Here, we plotted the trajectory of six stars of LD64k. All of them have escaped from the cluster by 3Myrs, as can be seen from the separation of black and red curves. One would imagine that their orbits do not evolve once they have escaped from the cluster. However, actually these stars "follow" the spiral-in of the cluster remnant. This behavior occurs due to the 1:1 resonance with the IMBH formed in the cluster. These stars have a pericenter distance of less than 0.1pc at the end of the simulation.

In figure 6, stars R1-R4 were brought to the GC by the 1:1 mean motion resonance. Figure 7 shows the orbit of R1 in a rotating frame where the distance between the SMBH and IMBH is scaled to unity. Star R1 escaped from the cluster at $T \simeq 2.5$ Myr and was orbiting around the SMBH until $T \simeq 3.8$ Myr. At $T \simeq 3.8$ Myr, it was captured into the resonance. Its orbit was a horseshoe orbit for $T \simeq 3.8$ Myr to $T \simeq 5$ Myr. From $T \simeq 5$ Myr to $T \simeq 6.5$ Myr, the orbit of R1 is that of a retrograde quasi-satellite. After that, it escaped from the resonance. Stars R2 through R4 show similar behaviors. Their distances from the GC have become smaller by a factor of five or more while they are in the resonance with the IMBH. Some of them escape from the resonance on the way to the GC.

Some stars are scattered by the IMBH during the resonance and change their orbit into those approaching the GC. We categorized such stars into a Resonance and Scatter group (RS), and show one example in figure 6. In this case, its semi-major axis does not decrease gradually, but suddenly through close encounters with the IMBH (see figure 6, middle-bottom panel). These resonant stars (R and RS) make up more than 90 % of stars whose pericenter distances, $r_{\rm p}$, are less than 0.5 pc from the GC (Table 7).

The right-bottom panel in figure 6 shows the orbital evolution of a star which escaped from the star cluster by a slingshot occurring in the star cluster. We categorized such stars into a Slingshot group (S). Some of them come very close to the GC. Moreover, these stars have very high inclinations (some have retrograde orbits) to the orbital plane of the star cluster because the escape direction from the star cluster is isotropic. They may be the origin of the stars which have high inclinations in the GC. Table 7 summarizes these results. We can see that the 1:1 resonance with the IMBH is the main mechanism which brings the stars close to the GC.

Figure 8 shows the cumulative number of escaped stars as a function of pericenter distance at the end of simulations. Solid curves include all stars and dashed curves only massive stars ($> 20M_\odot$). Dotted curves show the expected number of stars if the fraction of stars is independent of $r_{\rm p}$. We can see that there is a much larger number of massive stars in the central sub-parsec region than expected from the initial mass function.

In the case of run LD64k, there are 16 massive stars ($m > 20M_\odot$) with the pericenter distance less than 0.5 pc. Five of the 16 stars reached within 0.2 pc and three reached within 0.1 pc (see table 8). More than 10 % of stars with $r_{\rm p} < 0.5$ pc have masses $20M_\odot$. If the distribution of stars does not depend on their masses, the expected number of massive stars for the radius of 0.1pc is around 0.3. If there is no mass-dependent evolution effect, the chance that we find more than three stars with $r_{\rm p} < 0.1$ pc is 10^{-3}. In the other cases, a few persent of stars near the GC was massive at $r_{\rm p} = 0.5$ (pc) and the fraction is higher at more deeper region. In the initial mass function, only 0.5% stars have mass more than $20M_\odot$ and $\sim 0.1\%$ after runaway collisions because many massive stars are used up for the formation of the IMBH.

Figure 8 also shows that the number of the Trojan stars depends both on the mass of IMBH and the spiral-in timescale of IMBH. The number of resonant stars decreases when the IMBH mass is smaller. However, as the IMBH spirals in towards the GC in 5-6 Myrs, the number of Trojan stars is

not much different from that in our standard run (LD64k).

These results imply that star clusters selectively carry massive stars close to the GC. Massive stars sink to the center of their parent star clusters due to the mass segregation, while the stripping by the tidal force removes less massive stars from the outskirts of star clusters. As a result, massive stars tend to remain in star clusters and are carried to a few parsec from the GC before they escape from the cluster. Slingshot stars also include many massive stars because slingshots occur at the center of the star cluster where massive stars are gathering. Thus, star cluster scenarios can naturally explain why massive stars lie within the central parsec.

3.3. The Remnant of the Core and IRS 13E

At the end of the simulation, only one massive star is bound to the IMBH. However, several stars were bound till $T = 6$ Myrs for LD64k. These bound stars look like IRS 13E, which is located at $\sim$ 0.13 pc in projection from the GC and contains half a dozen massive and young stars within $\sim$ 0.01 pc. Because of their very similar proper motions, it has been suggested that they are bound to an IMBH and IRS 13E is the remnant of a star cluster containing an IMBH with $\sim 10^4 - 10^5 M_\odot$ (Hansen & Milosavljević 2003; Maillard et al. 2004). Figure 9 shows the proper motion of stars bound to the IMBH at $T = 4.62$ Myr for LD64k. The tidal radius is 0.15 pc and larger than the frame, but a few stars are within 0.01 pc. This is similar to the observation of the IRS 13E (see figure 2 in Maillard et al. 2004).

4. Summary

Using N-body simulation, we showed that many young and massive stars are carried to the GC by a star cluster due to the 1:1 mean motion resonance with an IMBH which is formed in the cluster. In addition, we found that slingshots in the star cluster throw stars into orbits which pass near the GC. These orbits have very high inclinations and are sometimes retrograde orbits. They are new channels which carry young stars to the central parsec. Our simulation demonstrated the existence of massive stars and we explained why they form a disk-like structure. The possible existence of two counter-rotating disks might suggest that two clusters have spiraled in. The interaction and resonance between stars and IMBHs from multiple clusters might be responsible for the existence of stars which are very close to the central SMBH.

The authors thank Takeru Suzuki for the data of very massive stars, Eiichiro Kokubo and Yusuke Tsukamoto for helpful discussions, and the referee, Stefan Harfst, for useful comments on the manuscript. M. F. is financially supported by Research Fellowships of JSPS for Young Scientists. This research is partially supported by the Special Coordination Fund for Promoting Science and Technology (GRAPE-DR project), Ministry of Education, Culture, Sports, Science and Technology, Japan. Part of calculations were done using the GRAPE system at the Center for Computational Astrophysics (CfCA) of the National Astronomical Observatory of Japan.

REFERENCES

Belkus, H., Van Bever, J., & Vanbeveren, D. 2007, ApJ, 659, 1576

Castor, J. I., Abbott, D. C., & Klein, R. I. 1975, ApJ, 195, 157

Chandrasekhar, S. 1943, ApJ, 97, 255

Eisenhauer, F., et al. 2005, ApJ, 628, 246

Fabian, A. C., Pringle, J. E., & Rees, M. J. 1975, MNRAS, 172, 15P

Freitag, M., Gürkan, M. A., & Rasio, F. A. 2006, MNRAS, 368, 141

Fryer, C. L., Woosley, S. E., & Heger, A. 2001, ApJ, 550, 372

Fujii, M., Funato, Y., & Makino, J. 2006. PASJ, 58, 743

Fujii, M., Iwasawa, M., Funato, Y., & Makino, J. 2007, PASJ, 59, 1095

Fujii, M., Iwasawa, M., Funato, Y., & Makino, J. 2008, ApJ, in press

Gaburov, E., Lombardi, J. C., & Portegies Zwart, S. 2008, MNRAS, 383, L5

Gayley, K. G. 1995, ApJ, 454, 410

Genzel, R. et al. 2003, ApJ, 594, 812

Gerhard, O. 2001, ApJ, 546, L39

Gürkan, M. A., & Rasio, F. A. 2005, ApJ, 628, 236

Hansen, B. M. S., & Milosavljević, M. 2003, ApJ, 593, L77

Heger, A., Fryer, C. L., Woosley, S. E., Langer, N., & Hartmann, D. H. 2003, ApJ, 591, 288

Hurley, J. R., Pols, O. R., & Tout, C. A. 2000, MNRAS, 315, 543

Ishii, M., Ueno, M., & Kato, M. 1999, PASJ, 51, 417

Kim, S. S., & Morris, M. 2003, ApJ, 597, 312

Kim, S. S., Figer, D. F., & Morris, 2004, ApJ, 607, L123

Kinoshita, H., Yoshida, H., & Nakai, H. 1991, Cel. Mech. and Dyn. Astr., 50, 59

Krabbe, A., et al. 1995, ApJ,

Levin, Y. & Beloborodov, M. 2003, ApJ, 590, L33, 447, L95

Lu, J. R., Ghez, A. M., Hornstein, S. D., Morris, M., Matthews, K., Thompson, D. J., & Becklin, E. E. 2006, Journal of Physics Conference Series, 54, 279

Makino, J., Fukushige, T., Koga, M., & Namura, K. 2003, PASJ, 55, 1163

Maillard, J. P., Paumard, T., Stolovy, S. R., & Rigaut, F. 2004, A&A, 423, 155

Mapelli, M., Hayfield, T., Mayer, L., & Wadsley, J. 2008, arXiv:0805.0185

Marigo, P., Chiosi, C., & Kudritzki, R.-P. 2003, A&A, 399, 617

McMillan, S. L. W., McDermott, P. N., & Taam, R. E. 1987, ApJ, 318, 261

Meurs, E. J. A., & van den Heuvel, E. P. J. 1989, A&A, 226, 88

Nayakshin, S., Cuadra, J., & Springel, V. 2007, MNRAS, 379, 21

Hobbs, A., & Nayakshin, S. 2008, arXiv:0809.3752

Owocki, S. P., Gayley, K. G., & Shaviv, N. J. 2004, ApJ, 616, 525

Paumard, T., et al. 2006, ApJ, 643, 1011

Portegies Zwart, S. F., Makino, J., McMillan, S. L. W., & Hut, P. 1999, A&A, 348, 117

Portegies Zwart, S. F., & McMillan, S. L. W. 2002, ApJ, 576, 899

Portegies Zwart, S. F., McMillan, S. L. W., & Gerhard, O. 2003, ApJ, 593, 352

Portegies Zwart, S. F., Baumgardt, H., Hut, P., Makino, J., & McMillan, S. L. W. 2004, Nature, 428, 724

Press, W. H., & Teukolsky, S. A. 1977, ApJ, 213, 183

Salpeter, E. E. 1955, ApJ, 121, 161

Suzuki, T. K., Nakasato, N., Baumgardt, H., Ibukiyama, A., Makino, J., & Ebisuzaki, T. 2007, ApJ, 668, 435

Wisdom, J. & Holman, M. 1991, AJ, 102, 152

Yungelson, L. R., van den Heuvel, E. P. J., Vink, J. S., Portegies Zwart, S. F., & de Koter, A. 2008, A&A, 477, 223

This 2-column preprint was prepared with the AAS LaTeX macros v5.2.

Table 1: Models for the galaxy

	King W_0	N	$M_{\rm G}({\rm M}_\odot)$	$m({\rm M}_\odot)$	$M_{\rm BH}({\rm M}_\odot)$	$r_{\rm h}$ (pc)
GL	10	2×10^6	5.8×10^7	29	3.6×10^6	22
GS	10	2×10^6	2.9×10^7	15	3.6×10^6	9.6

Table 2: Models for the star cluster

	King W_0	N	$M_{\rm SC}({\rm M}_\odot)$	$r_{\rm c}$ (pc)	$r_{\rm h}$ (pc)	$r_{\rm t}$ (pc)
SC64k	6	65536	2.0×10^5	5.9×10^{-2}	1.6×10^{-1}	1.1
SC32k	6	32768	1.0×10^5	3.5×10^{-2}	9.6×10^{-2}	6.5×10^{-1}

Table 3: Parameters

	$\epsilon_{\rm SC}$ (pc)	$\epsilon_{\rm G}$ (pc)	$\epsilon_{\rm SC-BH}$ (pc)	$\epsilon_{\rm G-BH}$ (pc)	$\Delta t_{\rm tree}$ yr
P1	0.0	4.9×10^{-2}	2.5×10^{-2}	2.5×10^{-1}	2.4×10^2
P2	0.0	2.3×10^{-2}	2.4×10^{-2}	2.4×10^{-1}	1.1×10^2

Table 4: Runs for isolated star clusters

	$\dot{m}$	$r_{\rm coll}$	$M_{\rm IMBH}(M_\odot)$	$M_{\rm lost}(M_\odot)$
LD	Low[1]	Double[3]	1.8×10^4	2.9×10^3
LS	Low	Single[4]	1.4×10^4	2.0×10^3
HD	High[2]	Double	8.3×10^3	9.0×10^3
HS	High	Single	6.7×10^3	6.8×10^3

[1] $\dot{m}=9.7\times10^{-8}m$ ($M_\odot$/yr)
[2] $\dot{m}=5.0\times10^{-7}m$ ($M_\odot$/yr)
[3] $r_{\rm coll}=r_1+r_2$
[4] $r_{\rm coll}=2(r_1+r_2)$

Table 5: Runs

	Galaxy	Star cluster	$\dot{m}$	$r_{\rm coll}$	Parameter	R_0 (pc)
LD64k	GL	SC64k	Low[1]	Double[3]	P1	12.5
HS64k	GL	SC64k	High[2]	Single[4]	P1	12.5
LD32k	GS	SC32k	Low	Double	P2	5
HS32k	GS	SC32k	High	Single	P2	5

[1] $\dot{m}=9.7\times10^{-8}m$ ($M_\odot$/yr)
[2] $\dot{m}=5.0\times10^{-7}m$ ($M_\odot$/yr)
[3] $r_{\rm coll}=r_1+r_2$
[4] $r_{\rm coll}=2(r_1+r_2)$

Table 6: Results

	$t_{\rm IMBH}$(Myr)	$M_{\rm IMBH}(M_\odot)$	$M_{\rm lost}(M_\odot)$	$t_{\rm dis}$[1] (Myr)
LD64k	2.6	1.6×10^4	2.4×10^3	5.3
HS64k	2.6	6.3×10^3	6.5×10^3	4.3
LD32k	2.3	8.8×10^3	1.5×10^3	2.7
HS32k	2.2	3.0×10^3	4.1×10^3	1.7

[1] Disruption time of star clusters, when the number of bound stars becomes less than ten.

Table 7: The number of stars within 0.5 pc for LD64k.

Pericenter distance	Bound	Slingshot	Resonance	Resonance & Scatter	total
$r_{\rm p}<0.5$ pc	2	27	280	45	354
$r_{\rm p}<0.2$ pc	0	4	52	0	56
$r_{\rm p}<0.1$ pc	0	0	23	0	23

Table 8: The number of massive stars within 0.5 pc for LD64k.

Pericenter distance	Bound	Slingshot	Resonance	Resonance & Scatter	Total
$r_{\rm p}<0.5$ pc	1	5	7	3	16
$r_{\rm p}<0.2$ pc	0	1	4	0	5
$r_{\rm p}<0.1$ pc	0	0	3	0	3

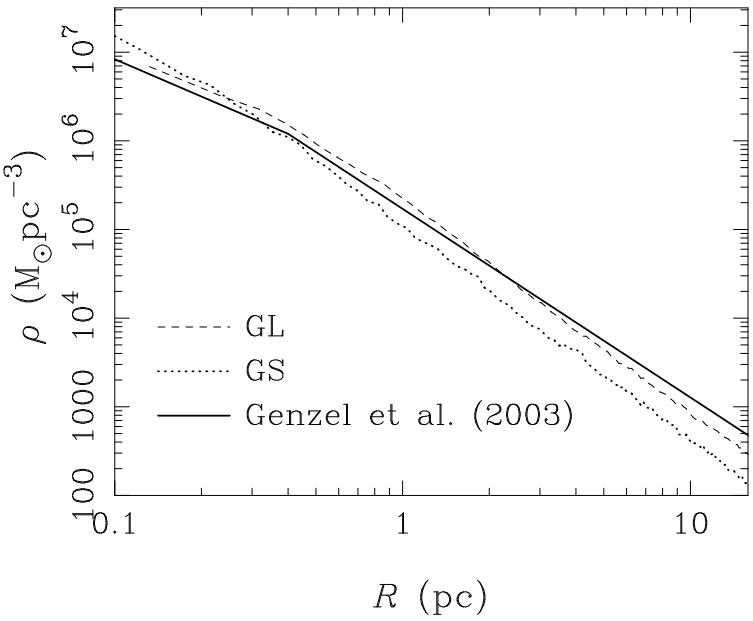

Fig. 1.— Density profiles for our models and the Galactic center (Genzel et al. 2003).

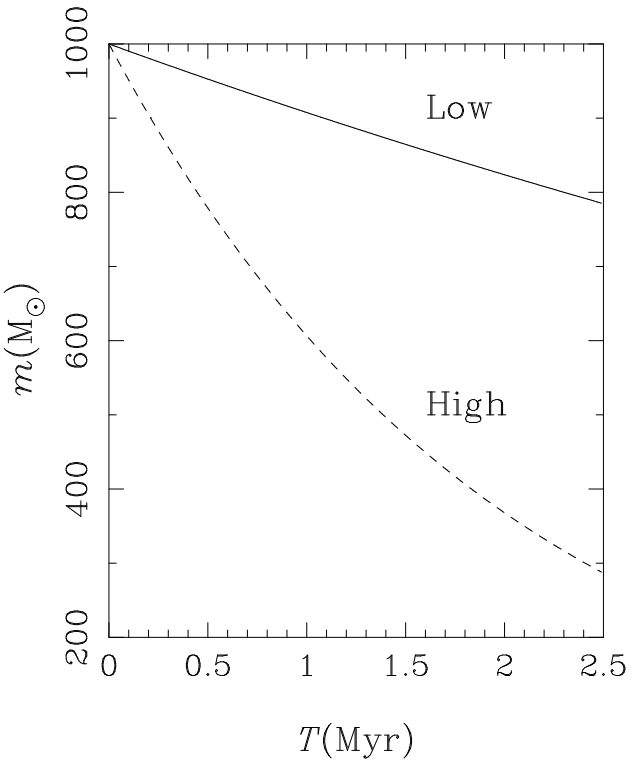

Fig. 2.— Evolution of the mass for stars with initial mass = $1000M_{\odot}$. The solid and dashed curves are the results with low mass-loss rate (see equation (3) in the text) and high mass-loss rate (five times as that of equation (3)), respectively.

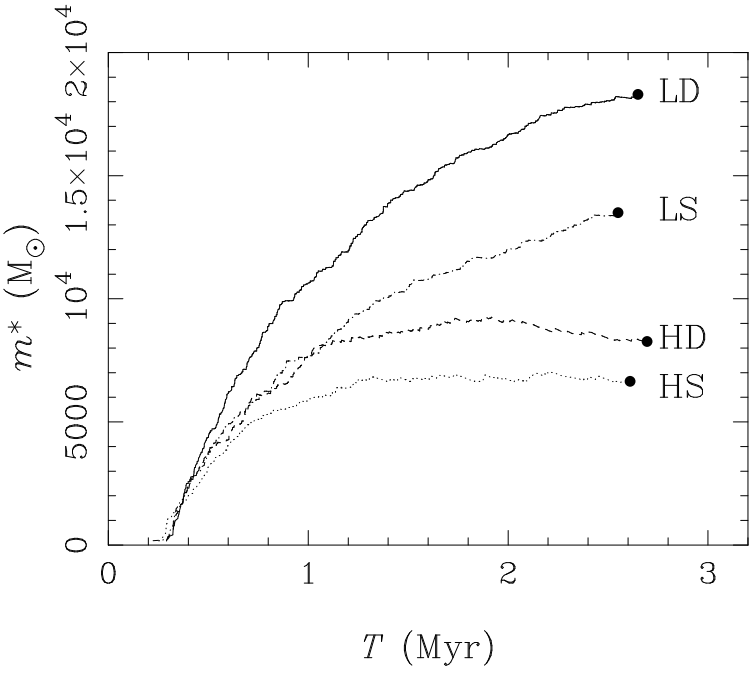

Fig. 3.— Evolution of the most massive star in the star cluster. The model of star cluster is SC64k. Black points show the time when IMBHs formed. "L" and "H" mean low- and high-mass loss rates, and "D" and "S" denote the collision radius. See table 4 for details.

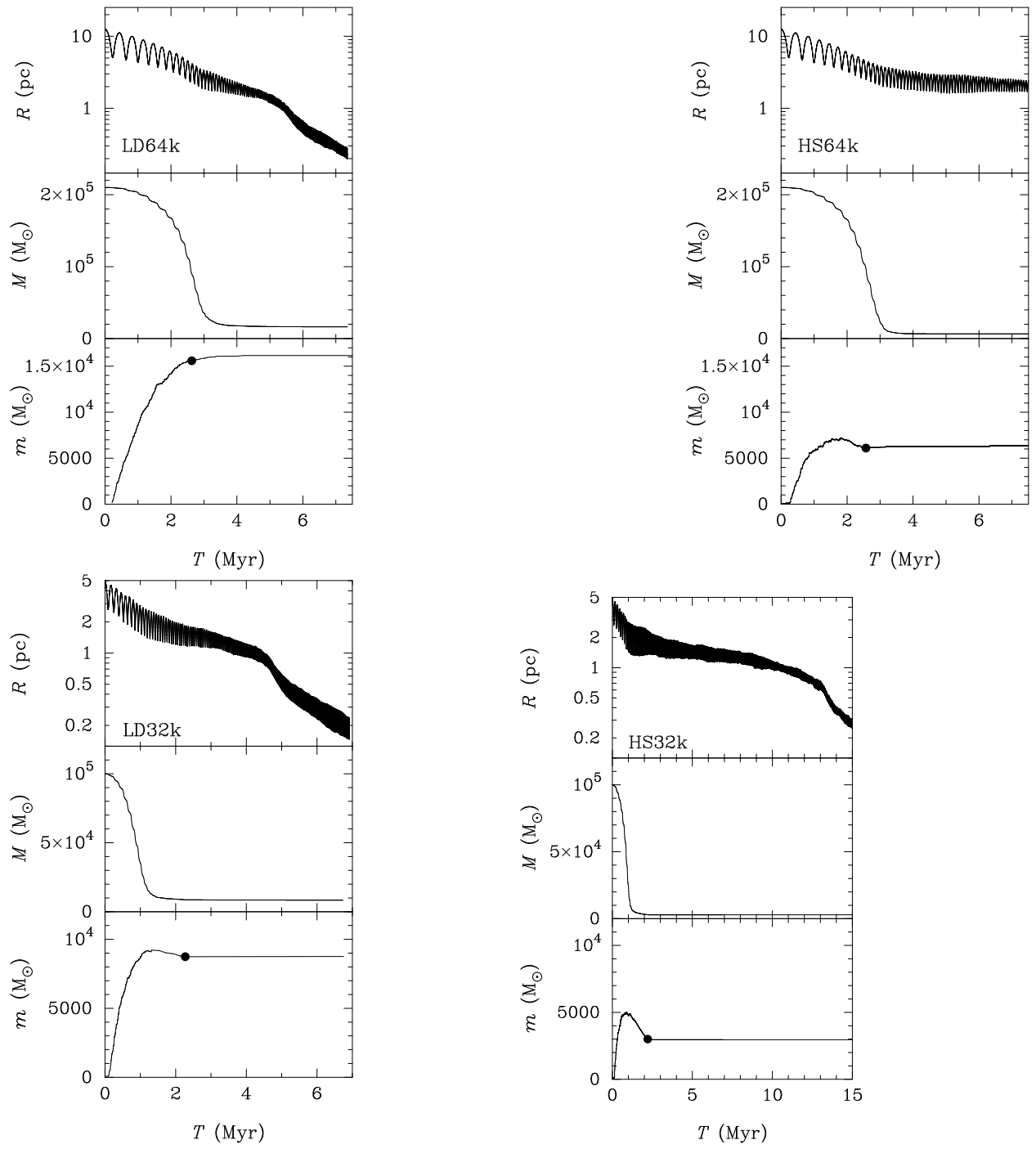

Fig. 4.— Evolution of star clusters. Top and middle panels show the orbital and bound-mass evolution of star clusters, respectively. Bottom panel shows the evolution of the most massive star in the star clusters. The black dot shows the time when the massive star became an IMBH.

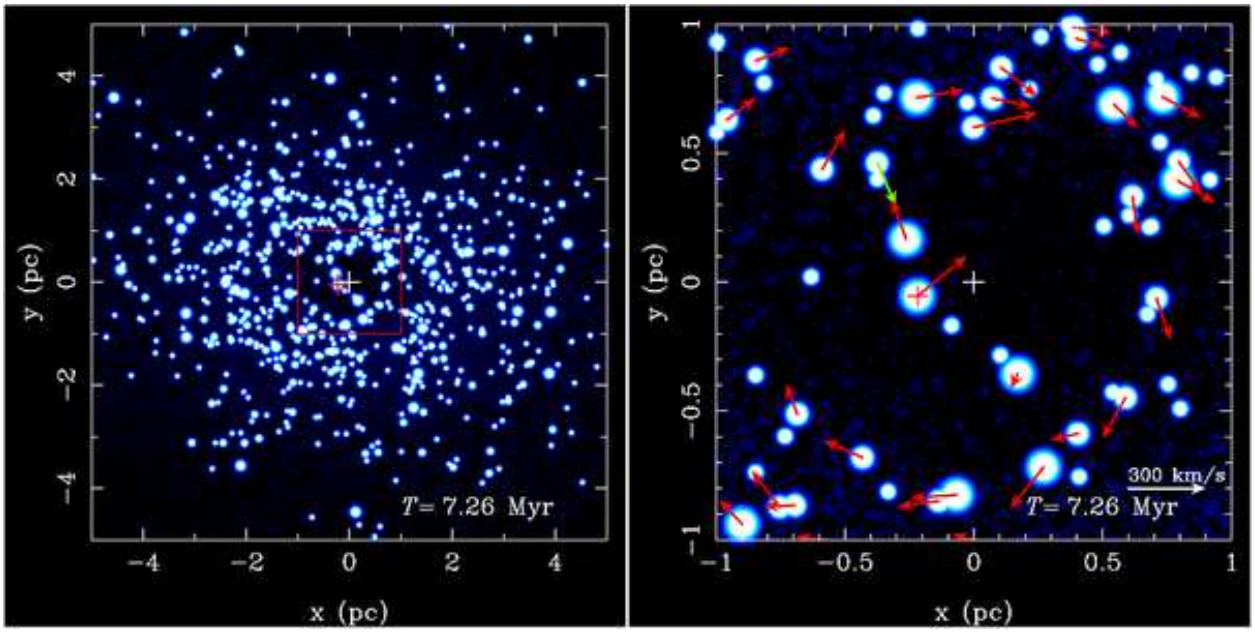

Fig. 5.— Projected distribution of stars at $T = 7.26$ Myr for LD64k. The orbital plane of the star cluster has an inclination of $i = 127°$ with respect to the plane of the sky, with a half-line of ascending nodes at $\Omega = 99°$ east of north. These values are used to mimic the result of Paumard et al. (2006). Right panel shows the central region shown by a red square in left panel. Arrows in right panel show the proper motion of stars. Red one shows clockwise orbit and green shows counter-clockwise. Red and white crosses show the positions of the IMBH and SMBH, respectively.

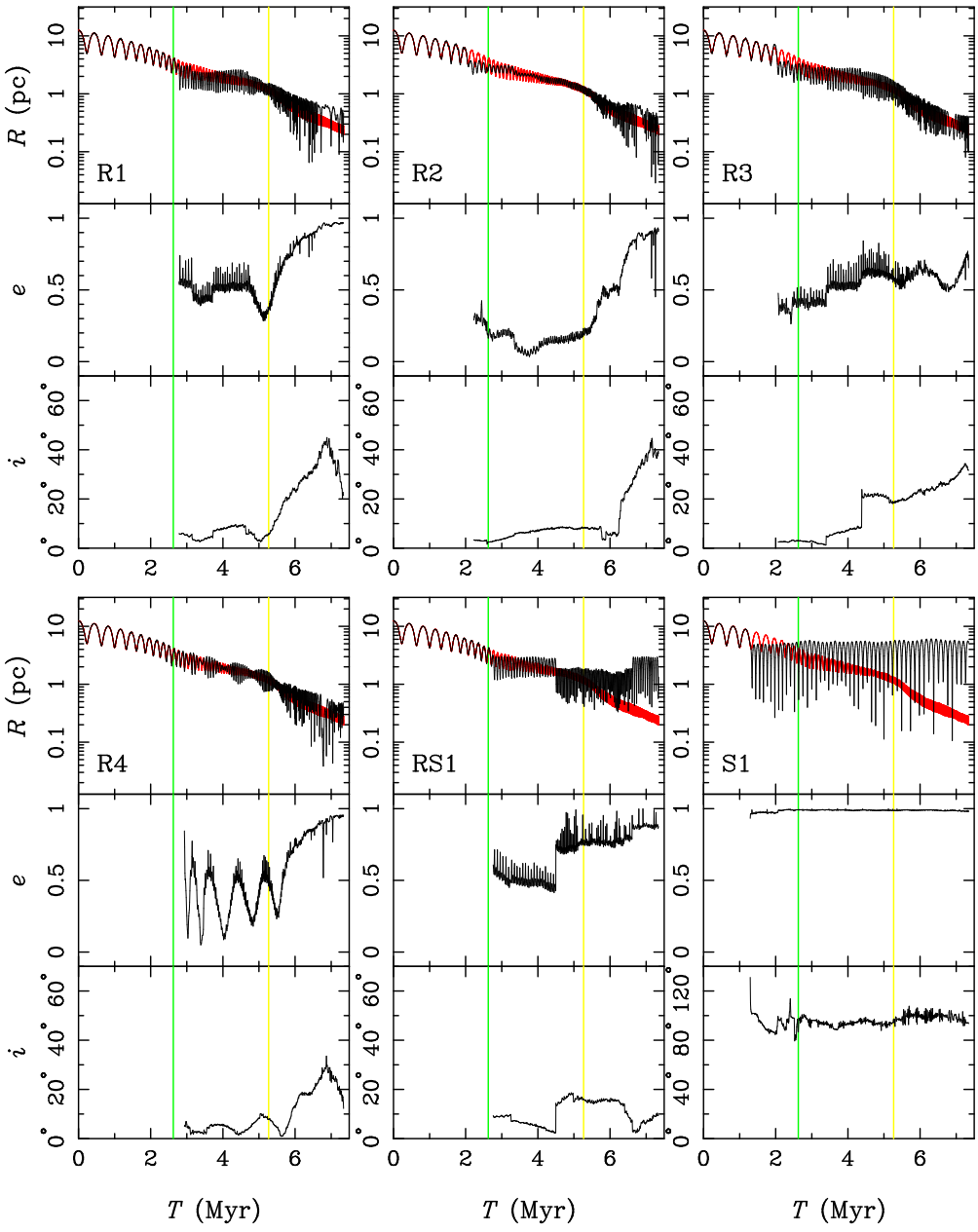

Fig. 6.— Evolution of position, eccentricities, and inclinations of stars escaped from the star cluster for LD64k. Red curve shows the orbital evolution of the star cluster or the IMBH formed in the cluster. Green and yellow lines show the time when the IMBH was formed and when the star cluster was disrupted (less than ten stars are bound to the cluster), respectively.

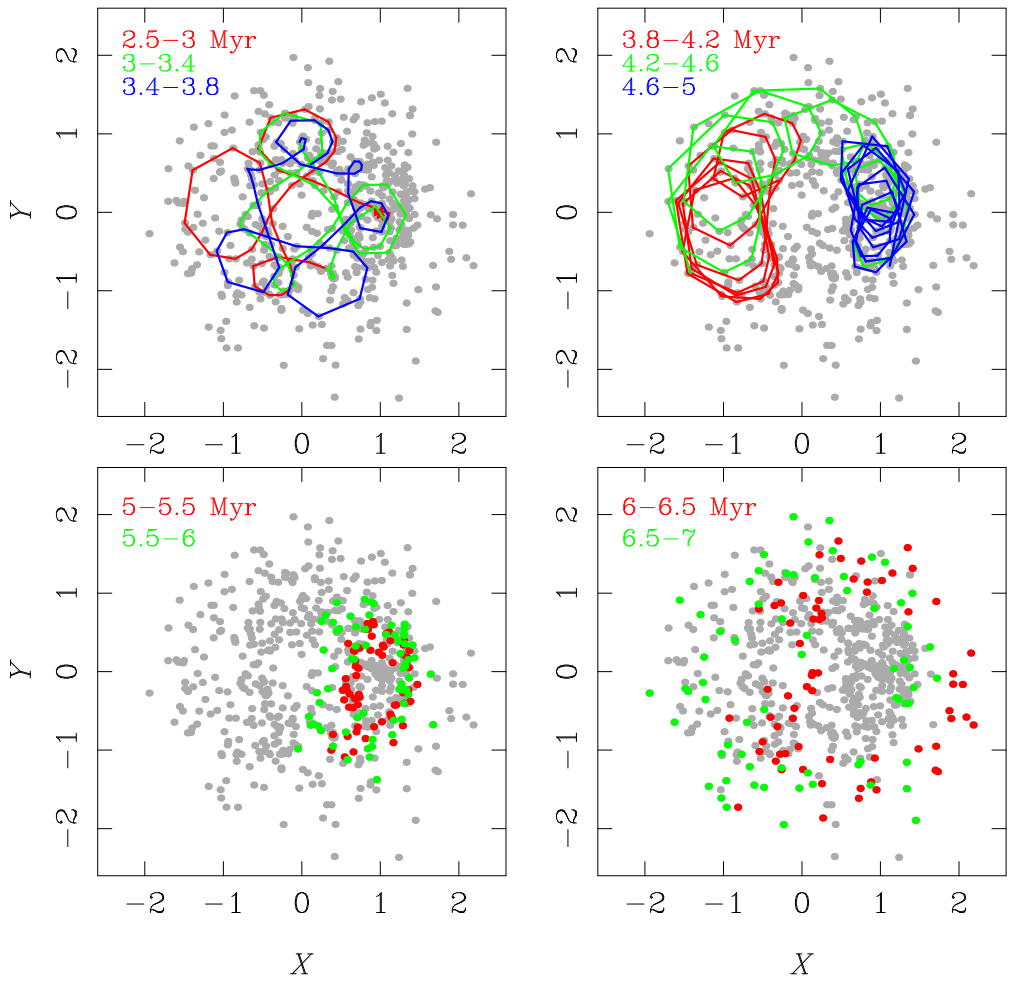

Fig. 7.— Orbit of star R1 in a rotational frame, where the IMBH is fixed at (1.0, 0.0). The SMBH lies on the origin. The distance of the star from the SMBH is normalized by the distance between the SMBH and the IMBH. Gray dots show all positions of the star obtained from snapshots. Colored curves or dots show the orbit or position of the star within time spans given in each panel.

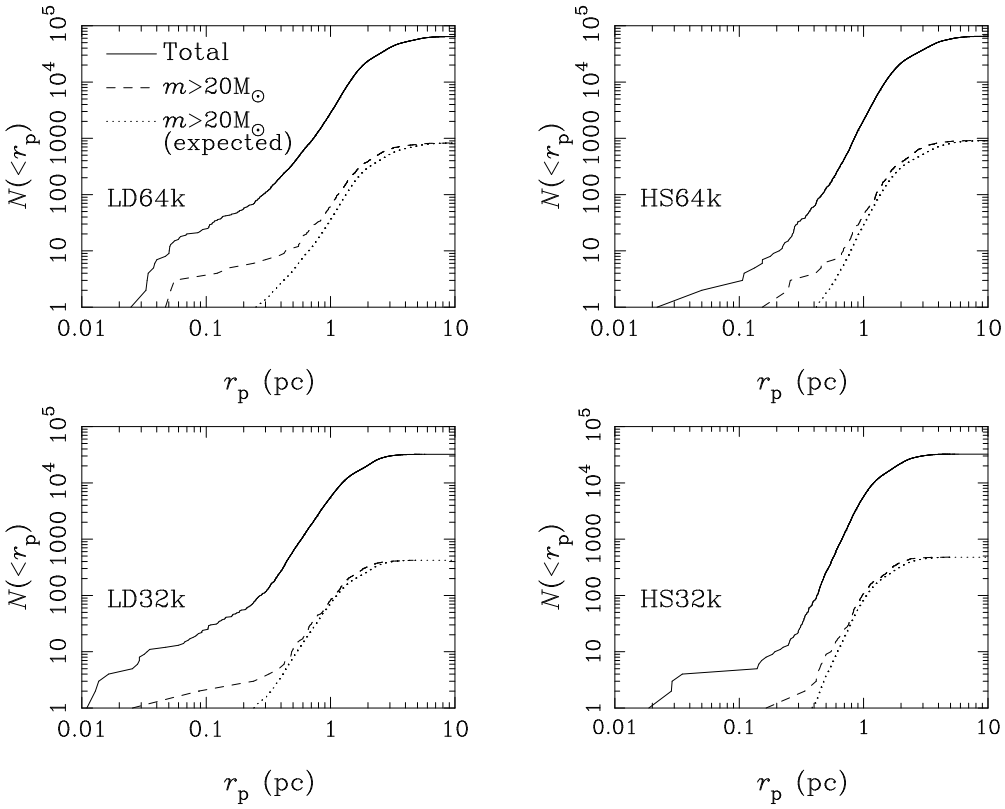

Fig. 8.— Cumulative number of escaped stars as a function of peri-center distance at the end of simulations. Solid curves include all stars and dashed curves only massive stars ($> 20M_\odot$). Dotted curves show the expected number of stars if the fraction of stars is the same, irrespective of $r_{\rm p}$.

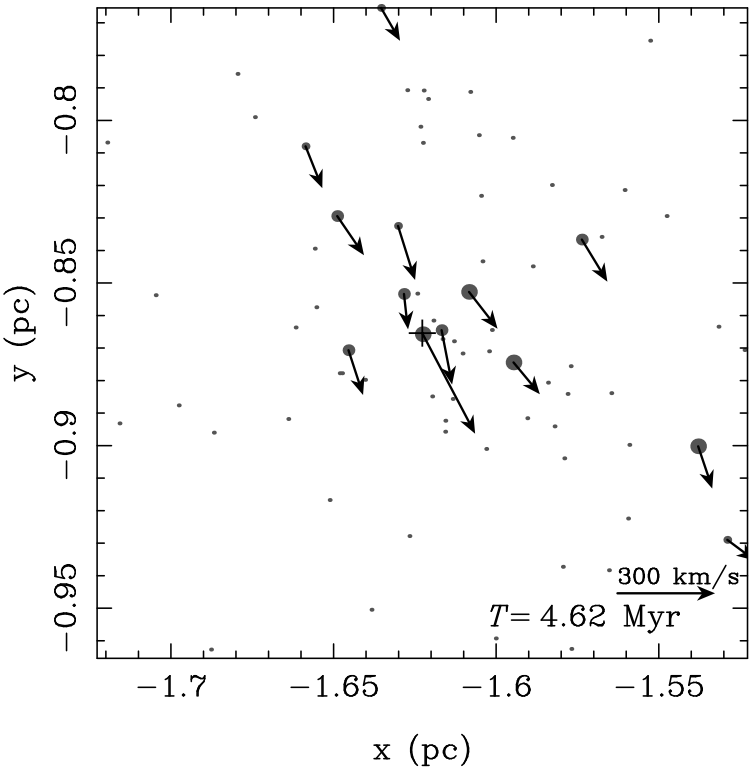

Fig. 9.— Snapshot of the remnant of the core. Vectors show the proper motion of stars for massive stars ($> 20M_{\odot}$). It is similar to IRS 13E (see figure 2 in Maillard et al. 2004).